Journal of Colloid and Interface Science 581 (2021) 895–904

Contents lists available at ScienceDirect

Journal of Colloid and Interface Science

journal homepage: www.elsevier.com/locate/jcis

Regular Article

Molecular structure of maltoside surfactants controls micelle formation and rheological behavior

Johan Larsson [a,*], Adrian Sanchez-Fernandez [b], Anna E. Leung [c], Ralf Schweins [d], Baohu Wu [e], Tommy Nylander [a,f], Stefan Ulvenlund [b,g], Marie Wahlgren [b,g]

[a] Physical Chemistry, Department of Chemistry, Lund University, Box 124, 221 00 Lund, Sweden
[b] Food Technology, Nutrition and Engineering, Lund University, Box 124, 221 00 Lund, Sweden
[c] European Spallation Source, Box 176, 221 00 Lund, Sweden
[d] Institut Laue-Langevin, DS / LSS, 71 Avenue des Martyrs, 38000 Grenoble, France
[e] Jülich Centre for Neutron Science (JCNS) at Heinz Maier-Leibnitz Zentrum (MLZ), Forschungszentrum Jülich GmbH, Lichtenbergstr. 1, 85748 Garching, Germany
[f] NanoLund, Lund University, Lund, Sweden
[g] Enza Biotech AB, Scheelevägen 22, 22363 Lund, Sweden

GRAPHICAL ABSTRACT

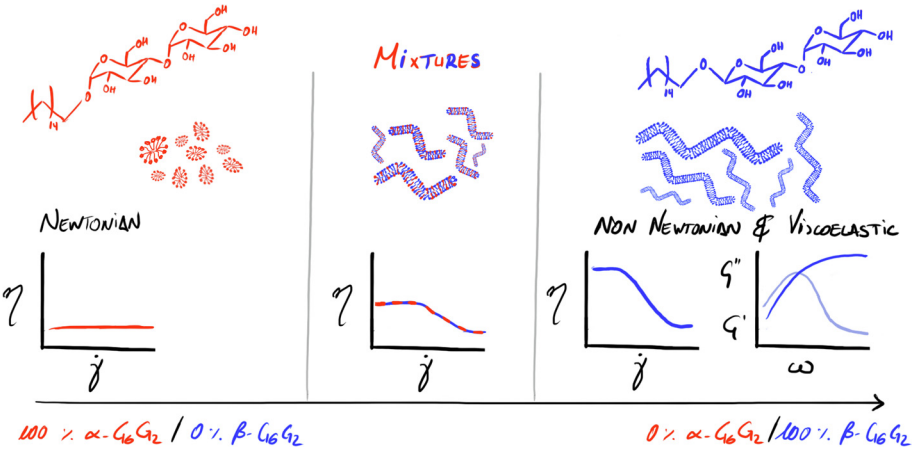

ARTICLE INFO

Article history:
Received 6 July 2020
Revised 27 August 2020
Accepted 28 August 2020
Available online 9 September 2020

Keywords:
Worm-like micelle
Viscoelastic
Sugar-based surfactant
Alkylglycoside
Rheology
Small-angle neutron scattering

ABSTRACT

Hypothesis: The anomeric configuration (α or β) of *n*-hexadecyl-D-maltopyranoside ($C_{16}G_2$) has been shown to affect the morphology of the micelle, from elongated for α-$C_{16}G_2$ to worm-like micelles for β-$C_{16}G_2$. The entanglement of worm-like micelles often leads to strong modifications of the rheological behavior of the system and, as such, the anomeric configuration of $C_{16}G_2$ could also provide the possibility of controlling this. Furthermore, mixing these surfactants are hypothesized to result in mixed micelles allowing to finely tune the rheology of a system containing these sustainable surfactants.
Experiments: The rheology of α- and β-$C_{16}G_2$, and mixtures of those, was determined by rotational and oscillatory rheology at different temperatures and surfactant concentrations. Micelle structure and composition for these systems were characterized using contrast variation small-angle neutron scattering and small-angle X-ray scattering. The results from these were connected in order to elaborate a molecular understanding of the rheological response of the system.
Findings: The self-assembly of these surfactants have been found to result in different rheological properties. β-$C_{16}G_2$ show a high viscosity with a non-Newtonian viscoelastic behavior, which was linked to

* Corresponding author.
E-mail address: johan.larsson@fkem1.lu.se (J. Larsson).

https://doi.org/10.1016/j.jcis.2020.08.116

the formation of worm-like micelles. In contrast, α-$C_{16}G_2$ self-assembled into short cylindrical micelles, resulting in a Newtonian fluid with low viscosity. Furthermore, mixtures of these two surfactants lead to systems with intermediate rheological properties as a result of the formation of micelles with intermediate morphology to those of the pure anomers. These results also show that the rheological properties of the system can be tuned to change the micelle morphology, which in turn depends on the anomeric configuration of the surfactant. Also, surfactant concentration, temperature of the system, and micelle composition for surfactant mixtures provide control over the rheological properties of the system in a wide temperature range. Therefore, these results open new possibilities in the development of sustainable excipients for formulation technology, where the characteristics of the system can be easily tailored through geometric variations in the monomer structure whilst maintaining the chemical composition of the system.

1. Introduction

A majority of surfactants used daily in e.g. detergents and as emulsifiers are produced from raw materials of fossil-based origin. As society moves towards more environmentally friendly products and processes, these surfactants need to be replaced with surfactants that are biodegradable and synthesized from renewable raw materials [1]. For this purpose alkylglycosides, which are surfactants with carbohydrate units as the hydrophilic headgroup, are particularly interesting and are therefore already used in applications like personal care products [2,3].

In previous work, we have demonstrated the formation of very elongated worm-like micelles (WLM) of the alkylglycoside *n*-hexadecyl-β-D-maltopyranoside (β-$C_{16}G_2$) and shown that the elongation was reduced substantially when changing to the anomer *n*-hexadecyl-α-D-maltopyranoside (α-$C_{16}G_2$) [4]. Here we will elaborate on the rheological behavior of these systems. It is well known that WLM behave as fluid thickeners, which is relevant for a range of products where surfactants are used. Among the most studied systems with WLM are ionic surfactants in salt solutions. These systems are sensitive to the ionic strength of the solution as the addition of salt modifies micelle morphology through screening the electrostatic repulsion between surfactant headgroups [5]. Some examples of ionic WLM are hexadecylpyridinium bromide in a sodium bromide solution [6], and sodium dodecylsulfate (SDS) in a NaCl solution [7]. A particular case is that of hydrotropic salts, which greatly modify the packing of surfactants through electrostatic screening and embedding hydrophobic domains into the micelle core. This is the case of hexadecyltrimethylammonium chloride in combination with sodium salicylate [8], and SDS with *p*-toluidine hydrochloride [9]. There are far fewer non-ionic surfactant systems that form WLM, and in most cases a co-surfactant is needed to obtain these structures [5]. One example where a co-surfactant is not required to form WLM is hexaethylene glycol hexadecyl ether ($C_{16}E_6$) [10]. Recently, very long WLM structures were also reported for a novel type of non-ionic surfactant, where the surfactant headgroup consists of a polyethylene glycol (PEG) linker with terminal carbohydrate units [11]. The formation of elongated micelles has also been reported for sugar-based surfactants, where the characteristics of those depend on the length of the hydrophobic tail and on the number of sugar units in the headgroup [12–14]. An advantage of non-ionic over ionic surfactants is that they are less sensitive to the salt concentration, generally less potent irritants and more environmentally friendly [15]. They can therefore be used in a wider range of formulated products [16].

WLM are elongated, dynamic surfactant self-assembled structures, which contain kinks, since a straight dynamic cylinder would be entropically unfavorable. Therefore, the contour length of the micelle (L) is much longer than the length of each rigid rod-like segment (the persistence length, l_p) [5]. A range of methods such as static and dynamic light scattering (SLS and DLS), small angle X-ray and neutron scattering (SAXS and SANS) and cryogenic transmission electron microscopy (cryo-TEM) are commonly used to reveal the hierarchical structure of these kinds of systems [5]. At low surfactant concentrations, the large distance between micelles precludes inter-micellar interactions, i.e. the solution is considered to be in the dilute regime. With increasing concentration, the number of WLM per unit volume increases and, in many cases, they also become longer [10]. This leads to shorter distances between micelles and at a threshold concentration (c^* or overlap concentration) they start to interact and entangle, defining the onset of the semi-dilute regime. Due to the length of the micelles this concentration is often very low for WLM (0.05–0.5 wt%). At c^* the viscosity (η) of the solution starts to increase and it behaves as a non-Newtonian fluid with increasing surfactant concentration, as a result of the collective motion of micelles [10].

The rheological behavior of WLM can be compared to that of polymers. As is commonly observed in polymer solutions, WLM solutions are most often shear thinning, meaning that the viscosity decreases with increasing shear rate (γ). This is due to an alignment of the micelles parallel to the flow [5]. When stress is applied, solutions of both WLM and polymer systems respond with a mode of relaxation called reptation, which is the diffusion along the length of the structure. The reptation time (τ_{rep}) is highly dependent on the contour length and scales with L [3,17]. While polymers are covalently bound and do not break, micelles are dynamic equilibrium self-assembly structures, meaning that they constantly break and reform. This gives WLM a second mode of relaxation, breaking time (τ_b), which makes their rheologic behavior different from that of polymers. The likelihood that a WLM breaks is the same for all parts of the micelle, which is why τ_b scales with L^{-1} [18]. These two relaxation modes respond differently to the micelle lengths. For shorter cylindrical micelles $\tau_{rep} \ll \tau_b$, the system behaves as polymers where reptation is the primary mode of relaxation. For WLM $\tau_b \ll \tau_{rep}$, Cates showed that the system can be described with a single relaxation time (τ) according to Equation (1) [19].

$$\tau = \sqrt{\tau_b * \tau_{rep}} \tag{1}$$

Under these conditions, a WLM system behaves as a Maxwellian fluid [20]. Thus, it can be considered to be viscoelastic, where at short timescales they behave as elastic solids and at longer timescales they behave as viscous liquids. τ is obtained by determining the frequency (τ^{-1}) at which the elastic modulus (G') and the viscous modulus (G") are equal. The viscoelastic behavior can be modelled with a Maxwellian model, where the G' and G" are described as in Equations (2) and (3) [21].

$$G' = G'_{\infty} \frac{(\omega\tau)^2}{1 + (\omega\tau)^2} \tag{2}$$

$$G'' = G'_{\infty}\frac{\omega\tau}{1+(\omega\tau)^2} \quad (3)$$

Here, ω is the angular frequency and G'_{∞} is the plateau value of G' at high frequencies. For Maxwellian fluids, it follows from the equations (2) and (3) that G'_{∞} is twice the value of the intersect between G' and G'' (from here on labelled as $G_{1/2}$). Several structural micellar dimensions, e.g. contour length, persistence length and distance between entanglements, can be estimated from rheological data [22].

In this work, the rheological properties of $C_{16}G_2$ will be discussed in relation to molecular and self-assembly structure of the surfactant. The static and dynamic rheology of the surfactant in its two anomeric configurations (α- and β-$C_{16}G_2$) and mixtures of those is probed at different temperatures and concentrations. The molecular organization of these surfactants was investigated using SAXS and contrast variation SANS. The rheology of these systems was then linked to the micellar structure observed in each case, thus connecting the macroscopic response of the system to the molecular organization of the surfactants.

2. Experimental section

2.1. Materials

n-Hexadecyl-α-D-maltopyranoside (α-$C_{16}G_2$) was purchased from Ramidus AB (Lund, Sweden) and *n*-hexadecyl-β-D-maltopyranoside (β-$C_{16}G_2$) was purchased from Anatrace Inc. (Maumee, Ohio). The structure of these surfactants is presented in Fig. S1 in the ESI. The purity of both surfactants was stated to be ≥97% by the suppliers and was verified by HPLC spectroscopy in this work. Tail-deuterated β-$C_{16}G_2$ (d_{31}-β-$C_{16}G_2$, 98.5 ± 2.0%D) was synthesized by the Deuteration and Macromolecular Crystallisation DEMAX platform (ESS, Sweden) according to the procedure in the ESI [23]. The purity and deuteration of the surfactant were assessed by ^{1}H (Figs. S2 and S3) and ^{13}C NMR spectroscopy (Figs. S4 and S5), and mass spectrometry. The water used in this work was of Milli-Q purity and the D_2O was purchased from Sigma Aldrich (Darmstadt, Germany) and was of 99.9 atom % D.

2.2. Methods

2.2.1. Sample preparation

The Krafft point of $C_{16}G_2$ is above room temperature (about 27 °C) [4]. Thus, to dissolve the surfactants, stock solutions were prepared under agitation at 45 °C until homogeneous solutions were obtained. Samples were prepared by diluting these stock solutions to the desired concentration and equilibrating at 45 °C prior to measurement. When dissolved at a temperature above its Krafft point, the surfactant does not precipitate from solution for at least 1 h at 25 °C, which provides enough time to characterize the assemblies in the kinetically arrested state below the Krafft point.

2.2.2. Rheology

The rheology experiments were performed on a Malvern Kinexus rheometer (Malvern Instruments limited, Worcestershire, UK). The data were analyzed using the software *rSpace for Kinexus* by Malvern Panalytical. The geometry used for the experiment was a 15.4 mm cup and a 14 mm cylinder. Complementary experiments were performed on a TA Instruments ARES rheometer (New Castle, USA). In this case, analysis of the data was done in the software *TA Orchestrator* and the geometry used was a 16.5 mm cylinder and 17 mm cup. The flow curves were recorded at a shear rate range of 0.01–300 s^{-1} with 7 measurements per decade. The linear viscoelastic region (LVER) was determined for each system, and subsequent experiments were conducted at a constant shear stress of 0.05 Pa over the frequency range 0.01–10 Hz. These conditions were such that every measurement was conducted in the LVER. The systems were equilibrated and analyzed at 30, 40, 50 and 60 °C.

The oscillatory rheology data were modelled using Maxwellian model fits, see Equations (2) and (3). As it proved difficult to estimate G'_{∞}, $2xG_{1/2}$ was used instead, keeping in mind that the equality $G'_{\infty} = 2xG_{1/2}$ is true for Maxwellian fluids only.

2.2.3. Dynamic light scattering (DLS)

The hydrodynamic radius (R_H) of the investigated systems was determined with a Zetasizer Nano-ZS (Malvern Instruments Ltd., Worshestershire, UK). The laser was a 4 mW He-Ne laser with a wavelength of 632.8 nm. Measurements were conducted in backscattering mode, with a scattering angle of 173°. The surfactant samples (0.5 ml, 10 mM) were injected in PMMA semi-micro disposable cuvettes purchased from BRAND GmbH (Wertheim, Germany) and analyzed from 70 °C to 10 °C with steps of 5 °C. Subsequent to any change in temperature the sample was equilibrated for 5 min and triplicates were measured for every point. Precipitation was detected at 20 °C and below for samples with high β-$C_{16}G_2$ ratios and results from such measurements were thus removed from the data set. Correlation functions showed a single exponential decay and data were analyzed with the Malvern Zetasizer software using the cumulants method.

2.2.4. Small angle X-ray and neutron scattering

Small angle X-ray scattering (SAXS) experiments were performed at the European Synchrotron Radiation Facility on the BM29 beamline (Grenoble, France). A wavelength of 0.99 Å and a sample-to-detector distance of 2.867 m were used, resulting in a Q range of 0.004–0.49 $Å^{-1}$, where Q is the scattering vector defined as $Q = 4\pi \sin\theta/\lambda$. Every sample was exposed to the beam for 10 frames of 1 s each and the final curve was obtained by averaging those frames for which beam damage was not observed. The samples were investigated at 25, 40 and 50 °C. The scattered intensity was converted to absolute scale according to the protocols of the beamline and the solvent contribution to the scattering was subtracted. The data output was absolute scattered intensity, I(Q), vs. scattering vector, Q [24].

Small angle neutron scattering (SANS) experiments were performed at the Institut Laue-Langevin (ILL) on the D11 instrument (Grenoble, France) [25] and at the Heinz Maier-Leibnitz Zentrum (MLZ) on the KWS-3 instrument (Garching, Germany) [26]. On D11, the neutron wavelength was 5.5 Å and the sample-to-detector distances were 1.65, 8 and 39 m resulting in a Q range of 0.0014–0.43 $Å^{-1}$, whereas on KWS-3 the wavelength of the neutrons was 12.8 Å, and two different sample-to-detector distances were used, 1.15 and 9.15 m, yielding a combined Q range of 0.00 0183–0.0187 $Å^{-1}$. The samples were injected in cylindrical quartz cuvettes ("banjo cells") with 1- and 2-mm path length for H_2O and D_2O samples respectively, and measured at 30 and 50 °C. The raw data were reduced according to the protocol of each beamline to obtain the output files in I(Q), in absolute intensity, vs. Q.

Analysis of the SAXS and SANS data was performed in SasView 4.2.2 by fitting to form factor models conforming to the micellar shape [27]. As the Q-range covered in the SAXS experiment did not reach sufficiently low-Q values to observe the longest dimension of the micelles, the model used for the SAXS data was a core–shell cylinder model describing the cross-section dimensions of the micelles. The SANS data were fitted with a flexible cylinder model, as these experimental data allowed the length and stiffness of the micelles to be determined. For a detailed description of the analysis of the SAXS and SANS data, see previous work [4].

3. Results

3.1. Structure-function coupling in α- and β-$C_{16}G_2$ micelles

The key results from the rheology measurements of α-$C_{16}G_2$ and β-$C_{16}G_2$ are summarized in Fig. 1. The linear rheology of these surfactants directly reveal significant differences between the two anomeric configurations when it comes to the magnitude of the viscosity and the flow curves (Fig. 1a). First, the viscosity is significantly lower for α-$C_{16}G_2$ and flow curves could only be recorded at high surfactant concentration and at a limited range of shear rates. Furthermore, α-$C_{16}G_2$ behaves as a Newtonian fluid where the viscosity does not vary with shear rate, while β-$C_{16}G_2$ shows a non-Newtonian behavior above 10 mM. At high concentration, the viscosity of β-$C_{16}G_2$ solutions decreases with increasing shear rate, i.e. the systems display a shear thinning behavior. The β-$C_{16}G_2$ solutions show an increase in viscosity with increasing surfactant concentration and, at the highest concentration studied (200 mM), the viscosity extrapolated to zero-shear (710 Pas) is more than six orders of magnitude higher than that of water at 50 °C (0.547×10^{-3} Pas) (Fig. 1b). The largest relative increase in viscosity with concentration is observed between 5 and 10 mM, i.e. at the concentration where the behavior of the system transforms from Newtonian to non-Newtonian. This change marks the onset of the semi-dilute regime, where the micellar-micellar interactions become the determining factor for the rheological behavior [20]. The observed interactions are expected to be relatively weak and therefore sensitive to the flow conditions, and this effect is more pronounced with increasing concentration (Fig. 1a). Interestingly, the flow curve for the most concentrated system (200 mM) shows a sharp discontinuity at 0.5 s^{-1}. This feature was confirmed to be reproducible in several independent experiments, using different instruments and configurations, and bears the character of a yield point. However, its physical underpinnings are not understood at the current point in time.

The zero-shear viscosity appears to increase in a sigmoidal fashion with concentration (Fig. 1b). The steepest increase is observed at surfactant concentration between 20 and 70 mM. In this range the viscosity shows a power law dependence on the surfactant concentration with an exponent of 5.52. This should be compared with the value of 5.8 observed for semi-dilute solutions of unbreakable polymers [28], indicating that, in this region, the fastest mode of relaxation for the micelles is reptation. For Maxwellian systems, where the micelles break much faster than they reptate along the contour length ($\tau_{break} \ll \tau_{rep}$), the power law exponent has been shown to be 3.7 for concentrations in the semi-dilute regime [28]. Indeed, when increasing the concentration of β-$C_{16}G_2$ above 70 mM, the exponent decreases to a value of 3.23. This indicates that the system goes through a transition around 70 mM, from which the dominant relaxation mode is reptation of intact micelles at lower concentration to fast-breaking micelles at higher concentration, where the system behaves as a Maxwellian fluid.

The rheological properties of the $C_{16}G_2$ system were further investigated by determining the viscoelastic properties at different frequency of oscillating strain (Fig. 1c–e). For β-$C_{16}G_2$, the viscous modulus (G") is dominating at low frequencies and the elastic modulus (G') is dominating at high frequencies, which is the expected behavior of a viscoelastic system. The τ value is obtained from the inverse of the angular frequency (ω) at the point where G"=G'. Both τ and $G_{1/2}$ increase with the surfactant concentration. This is expected, since an increase in surfactant concentration results in an increasing number of interacting micelles. Therefore, the solution shows a more elastic behavior over larger time scales and requires larger forces to make it flow [21]. The solid and dashed lines in Fig. 1c–e represent the fit of the Maxwell model to the experimental data. The model fits the data reasonably well at high concentrations (≥100 mM), but not at lower concentrations. This conforms with the results from the viscosity measurements discussed above. For the system to behave according to Maxwell's model, the micelles must be sufficiently long and entangled so that the relaxation through breaking the micelles is much faster than through reptation along its contour length and, consequently, only a single relaxation time of the system upon deformation is observed [19]. The fit to Maxwell's model is poor for G" at high frequencies. This is common for WLM systems, since at shorter time-scales additional relaxation mechanisms, for instance stretching of the micelles, which are not accounted for in the Maxwell model become significant [21].

The differences in the rheological behavior of α- and β-$C_{16}G_2$ anomers can be explained by the formation of different micellar structures, as confirmed by SANS. We found that α-$C_{16}G_2$ behaves as a Newtonian fluid, consistent with the previous report that this anomer forms elongated micelles that are not sufficiently long to confer the system non-linear response to stress, even at high surfactant concentration [4]. Scattering data show that β-$C_{16}G_2$ forms WLM [4], which in the semi-dilute regime correlates well with the non-linear response to stress, i.e. the shear thinning behavior of the system. In the present study, the morphology of α- and β-$C_{16}G_2$ is further investigated using a wider Q-range and over a wider range of concentrations. We note that the analysis of scattering data becomes challenging at higher surfactant concentrations (>10 mM), i.e. when reaching the semi-dilute regime for β-$C_{16}G_2$,

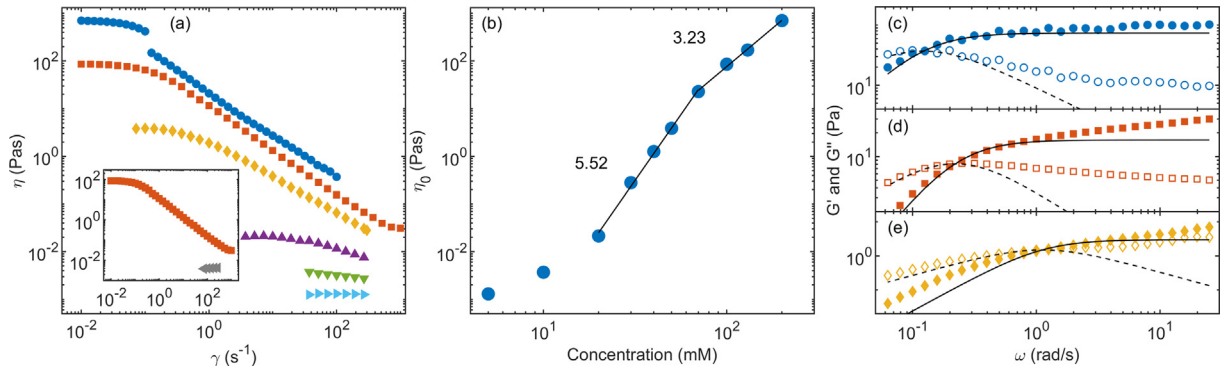

Fig. 1. Summary of the key results from rheology measurements of $C_{16}G_2$ at 50 °C. (a) Viscosity versus shear rate for β-$C_{16}G_2$ at 200 (○), 100 (□), 50 (◇), 20 (△), 10 (▽) and 5 (▷) mM surfactant concentration. The inset compares the viscosity for α-$C_{16}G_2$ (◁) and β-$C_{16}G_2$ (□) at 100 mM. (b) Zero-shear viscosity of β-$C_{16}G_2$ versus concentration where the slopes of two different regions are indicated using solid lines. Viscoelastic properties of β-$C_{16}G_2$ at (c) 200, (d) 100 and (e) 50 mM respectively as the G' (filled markers) and G" (unfilled markers) versus the angular frequency. The solid and dashed lines are the G' and G" Maxwell model fit of the data.

as it requires that the excluded volume effects due to intermicellar interactions are properly taken into account [29]. Therefore, the detailed investigation of the micelle morphology was performed in the dilute regime, i.e. at surfactant concentrations of 10 mM and below for β-$C_{16}G_2$. The dilute regime of α-$C_{16}G_2$ extends to higher concentrations since it is forming shorter micelles and, thus, a sample of 20 mM α-$C_{16}G_2$ was included in the analysis. SANS data and best fits of the flexible cylinder model for the anomerically pure samples are presented in Fig. 2a and in the ESI in Fig. S8, and the results from the fits are presented in Fig. 2c and d and in the ESI in Table S1.

The results of the SANS measurements at 50 °C revealed that α-$C_{16}G_2$ forms elongated micelles that have a contour length which is longer than their persistence length at all investigated concentrations. We also see an increase of contour length with increasing surfactant concentration, as expected for long-tailed surfactants in the dilute regime [10]. However, the contour length remains <2000 Å for all concentrations studied. For β-$C_{16}G_2$, on the other hand, formation of WLM with contour length >8000 Å is shown already at concentrations as low as 1 mM (Fig. S8 and Table S1). The length of the micelles seems to increase up to ~10000 Å at 5 mM surfactant. This type of micelle growth was also observed through the hydrodynamic radius determined by DLS as reported in the previous study [4]. An apparent decrease in the obtained contour length is observed at 10 mM. This is probably due to interactions between micelles at the onset of the semi-dilute regime, i.e. at the surfactant concentration c*. The observation is in line with results from the rheology measurements that also indicate onset of the semi-dilute regime at a surfactant concentration of 10 mM. A maximum in the apparent micelle size at c*, was also found by Jerke et al. for two other WLM systems [10]. They also show that if the structure factor is not taken into account, the flexible cylinder model overestimates the stiffness of the WLM. However, Chen et al. showed that even when the micellar interactions are considered, the stiffness of WLM increases with concentration [30]. This is also observed in the present study, where the persistence length increases with concentration in the dilute regime of β-$C_{16}G_2$-solutions (205 ± 10 Å at 1 mM, 273 ± 10 Å at 5 mM and 316 ± 10 Å at 10 mM). However, this variation in persistence length induced by concentration effects could be an artefact of the fitting approach, as the modelling underestimates the excluded volume effects. As previously reported, there is no major effect on the micelle cross-section with changes in concentration and the average micelle radius is 22.8 ± 0.2 Å for β-$C_{16}G_2$ and 20.4 ± 0.3 Å for α-$C_{16}G_2$ [4].

These results are in line with previous results for α- and β-$C_{16}G_2$, where the differences in the micelle morphology were attributed to changes in the mechanism of headgroup solvation between the two anomeric configurations [4]. The structure of the α anomer favored headgroup-solvent interactions, resulting in a higher degree of hydration than the β configuration and, thus, inducing a higher curvature and the formation of smaller micelles. The packing of the β anomer was instead driven by the stronger headgroup-headgroup attractive interactions, possibly through hydrogen bonds. This results in a more efficient packing of the headgroups, a lower degree of solvation, and the formation of larger aggregates.

3.2. Effect of temperature on the rheology and micellar structure

It has been previously shown that α-$C_{16}G_2$ undergoes a globular-to-elongated micelle morphology transition with temperature, while β-$C_{16}G_2$ forms WLM over the whole temperature and concentration range [4]. In connection to the distinct microscopic features of the micelles, the rheological behavior is affected by temperature. In this work we see that a Newtonian behavior is maintained over the whole temperature range investigated for 200 mM α-$C_{16}G_2$, meaning that the temperature-induced micellar growth is not extensive enough to induce a non-Newtonian behavior (Fig. S9). In contrast, the rheological behavior of β-$C_{16}G_2$ above 10 mM concentration was found to be non-Newtonian at all temperatures. The change in zero-shear viscosity with temperature for β-$C_{16}G_2$ is shown in Fig. 3a. For all concentrations the curves feature a maximum, where the highest viscosity extrapolated to zero-shear rate is achieved at temperatures between 40 and 50 °C. These zero-shear values were found to be lower at 30 °C and 60 °C by up to a factor of *ca.* 5 for 100 and 200 mM, and a factor of *ca.* 50 for 50 mM. Interestingly, the maximum in viscosity as a function of temperature is also concentration dependent, where it appears to occur at decreasing temperatures with increasing concentration.

The rheological behavior can be directly correlated to changes in micelle morphology. It is well-known that the microscopic structure and dynamics of micelles correlate to the macroscopic behavior of the system. For instance, longer micelles lead to higher viscosities, since the extent of entanglement increases with micellar length. Similarly, micellar flexibility has been shown to affect the entanglement of a micellar system and, thus, its rheology [20]. For the system studied here, the results from SANS measurements of 10 mM β-$C_{16}G_2$ at 30 °C and 50 °C show that the micelles are around 1000 Å shorter, but slightly more rigid at 30 °C, see

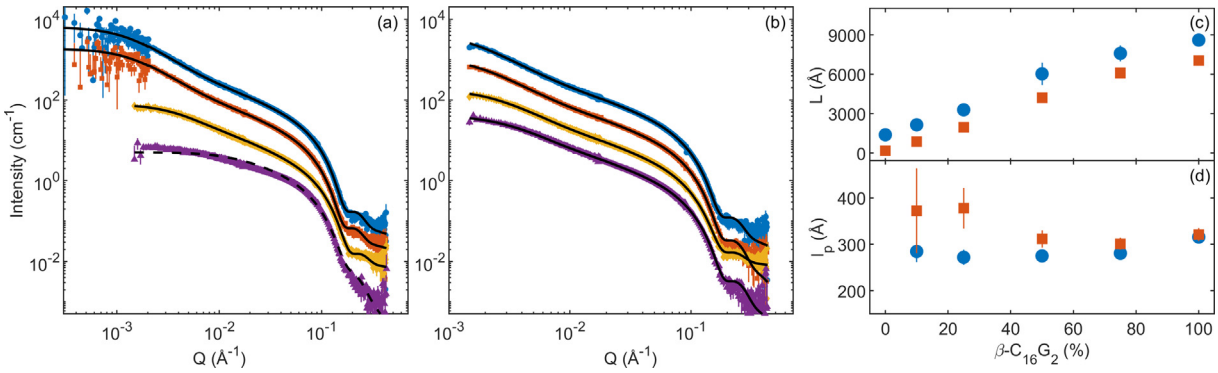

Fig. 2. SANS data for α- and β-$C_{16}G_2$ micelles at 10 mM in water. (a) β-$C_{16}G_2$ at 50 °C (blue ○) and 30 °C (red □) and α-$C_{16}G_2$ at 50 °C (yellow ◇) and 30 °C (purple △). (b) Mixtures of α- and β-$C_{16}G_2$ at: 75% (blue ○), 50% (red □), 25% (yellow ◇) and 10% (purple △) β-$C_{16}G_2$. Solid lines represent fits from a flexible cylinder model and dashed line represents fit from ellipsoid model. (c) Contour length, L, and (d) persistence length, l_p, obtained from flexible cylinder model fit of micelles at different mole % of β-$C_{16}G_2$ at 50 °C (○) and 30 °C (□). The intensity of the data and fits in (a) and (b) have been offset for clarity by a factor of 3, 10 and 30. (For interpretation of the references to color in this figure legend, the reader is referred to the web version of this article.)

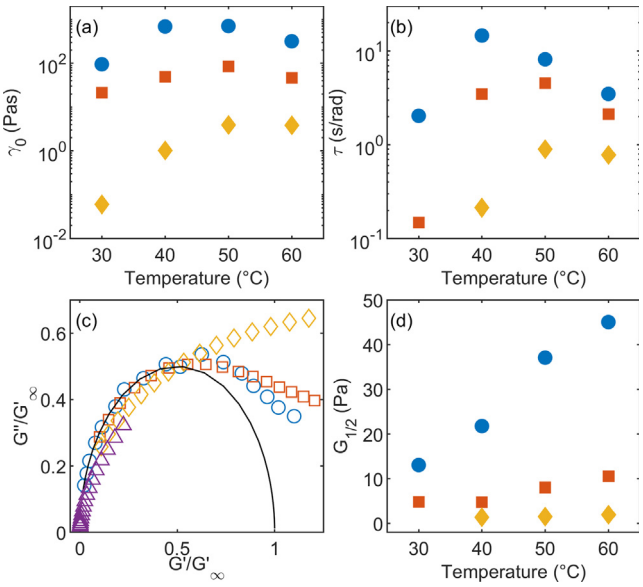

Fig. 3. The effect of temperature on the rheological behavior of β-$C_{16}G_2$ at 200 mM (○), 100 mM (□) and 50 mM (◇) surfactant concentration: (a) effect of zero-shear viscosity and (b) effect of relaxation time. (c) Normalized Cole-Cole plot for 100 mM β-$C_{16}G_2$ at 60 °C (○), 50 °C (□), 40 °C (◇) and 30 °C (△) with the solid line showing the Maxwell model fit. (d) The effect of temperature on the modulus at the intersection ($G_{1/2}$) of G' and G".

Fig. 2c and d. This is in agreement with previous investigations that showed that the hydrodynamic radius of the micelles, obtained from DLS measurements, goes through a maximum between 40 and 55 °C [4]. This, in turn, suggests that the system diverges from a Maxwellian behavior and explains the lower viscosity at zero-shear under these conditions. The increase in length of the micelles shows the same temperature trend as the zero-shear viscosity (Fig. 3a) indicating that the primary temperature effect on these values comes from the change in micelle length.

It is thus clear that the temperature dependence of the rheological properties reflects changes in micelle morphology. Interestingly, mean-field theory applied to these type of systems predicts a decrease in the micelle length with increasing temperature according to Equation (4) [22].

$$\bar{L} = \sqrt{\varphi}\exp\left(\frac{E}{2k_BT}\right) \quad (4)$$

Here $\bar{L}$ is the average length of the micelles, φ is the volume fraction of micelles, E is the scission energy and T is the temperature. The observed maximum in zero-shear viscosity with temperature reflects the sum of two effects, where transitions in viscosity are observed at different temperatures depending on the concentration.

The relaxation time behaves in a similar fashion to the zero-shear viscosity (Fig. 3b), where the τ values again show a maximum at temperatures between 40 °C and 50 °C, and this variation is also attributed to the morphological changes observed in the micelles. Furthermore, the temperature increase results in a more Maxwellian behavior, as evident in the normalized Cole-Cole plots for 100 mM β-$C_{16}G_2$ at different temperatures (Fig. 3c) (G" and G' are both normalized to G'_∞). Cole-Cole plots for 50 and 200 mM are shown in Fig. S10. The variation in the τ values, together with changes in the Maxwellian behavior, confirm that the individual components of the relaxation time (τ_{break} and τ_{rep}) are affected differently by temperature. Here, we hypothesize that the presence of longer, less mobile micelles (and thus an increase in τ_{rep}) is accompanied by an increase in micelle breakage (and thus a decrease in τ_{break}) [17,18]. Thus, we will reach a condition where $\tau_{break} \ll \tau_{rep}$ and the system becomes more Maxwellian with increasing temperature.

The modulus at the G'-G" intersect ($G_{1/2}$) is not affected by temperature changes in the same way as the zero-shear viscosity and the relaxation time (Fig. 3d). For Maxwellian WLM systems, it has been shown that G'_∞, and thus $G_{1/2}$, increase linearly with temperature [31], which is also the trend observed for β-$C_{16}G_2$ at 200 mM and for 100 mM above 40 °C. This confirms that the Maxwell regime starts around 100 mM at 40 °C, which is consistent with the previous results of zero-shear viscosity of β-$C_{16}G_2$ at different concentrations (Fig. 1b), that indicate the Maxwell model regime to start around 100 mM at this temperature.

It has previously been shown that α-$C_{16}G_2$ undergoes a globular-to-elongated micelle morphology transition with temperature, while β-$C_{16}G_2$ forms WLM over the whole temperature and concentration range [4]. This was again attributed to changes in the solvation mechanism, which were different for the two anomers. Whilst the solvation and, therefore, the morphology of β-$C_{16}G_2$ micelles remains relatively unaffected by temperature, the degree of solvation of α-$C_{16}G_2$ increases with decreasing temperature. This results in the formation of smaller aggregates of α-$C_{16}G_2$ at a lower temperature as induced by the increase in the apparent size of the α headgroup.

3.3. Mixtures of α-$C_{16}G_2$ and β-$C_{16}G_2$

α- and β-$C_{16}G_2$ display drastically different microscopic and macroscopic behavior. In terms of rheology, mixing the two surfactants results in solutions with intermediate viscosity between the two anomerically pure surfactants, where higher contents of the β anomer display higher viscosities (Fig. 4a). Similar to the concentration dependence of β-$C_{16}G_2$ in Fig. 1b, there is a weak sigmoidal dependence of zero-shear viscosity on the anomeric ratio, where the largest change is observed around 50% β-$C_{16}G_2$. As for β-$C_{16}G_2$, the mixtures are shear thinning, but the onset of the curve shifts to higher shear rates with increasing amount of α-$C_{16}G_2$ and becomes close to Newtonian at low β-$C_{16}G_2$ contents (<25%) (Fig. S11).

Large changes are also seen for the viscoelastic properties of the surfactant solutions when mixing α- and β-$C_{16}G_2$ (Fig. 4b-d). These oscillatory rheology results show that increasing amount of β-$C_{16}G_2$ in the mixture results in a more elastic solution, as seen by the shift of the intersection to lower angular frequencies. For mixtures with more than 50% α-$C_{16}G_2$ the viscous modulus is dominating over the whole frequency range investigated and no cross-over frequency could be detected. The temperature behavior of the mixtures with high ratios of β-$C_{16}G_2$ (>75%) is similar to that of pure β-$C_{16}G_2$. The τ decreases with increasing ratio of α-$C_{16}G_2$ meaning that the solutions are viscous over larger timescales (Fig. 4e). A maximum in τ appears at temperatures between 40 °C and 50 °C for the higher β-$C_{16}G_2$ ratios. At temperatures below 50 °C, $G_{1/2}$ is unaffected by changes in surfactant ratio. However, a significant increase is observed at higher temperatures for the systems with higher β-$C_{16}G_2$ ratio (Fig. 4f). Interestingly, such an increase is observed under conditions where a Maxwellian behavior is expected, as discussed earlier. The normalized Cole-Cole plot for the mixtures of α- and β-$C_{16}G_2$ is presented in Fig. 4g. Cole-Cole plots for the mixtures at all investigated temperatures are presented in Fig. S10. From the comparison of the curves, it is seen that the surfactant solution becomes more Maxwellian with increasing β-$C_{16}G_2$ ratio, as expected.

Again, the observed changes in rheological behavior can be related to the structural changes of the micelles. The hydrodynamic radius of the micelles, determined from DLS, shows a gradual increase in size with increasing ratio of β-$C_{16}G_2$ at constant

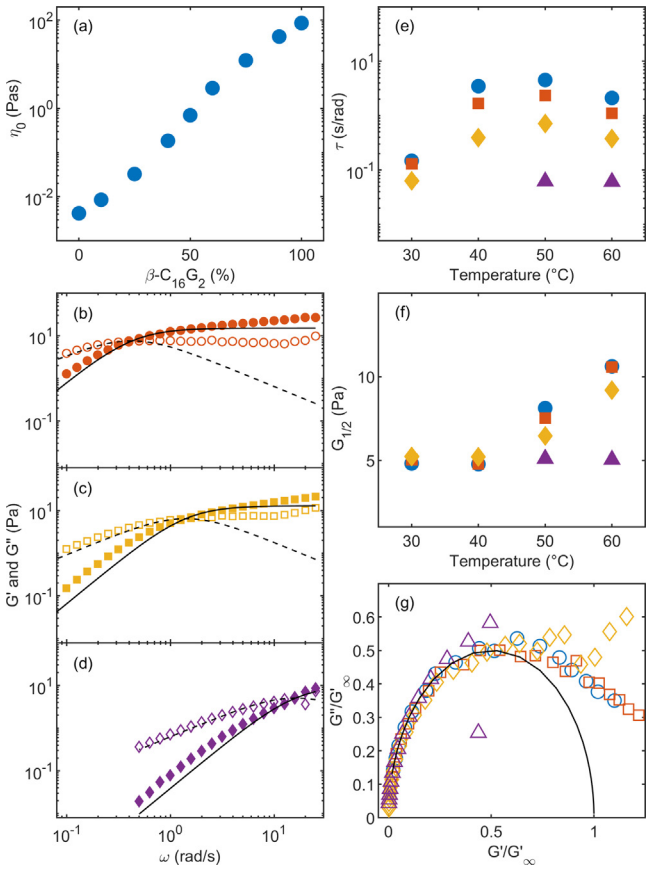

Fig. 4. Rheology results for mixtures of α- and β-$C_{16}G_2$ at 100 mM surfactant concentration. (a) Zero-shear viscosity at 50 °C. Frequency sweep measurements for (b) 90%, (c) 75%, (d) 50% β-$C_{16}G_2$, with G' (filled markers) and G'' (unfilled markers). Maxwell model fits are included for G' (solid line) and G'' (dashed line). Temperature dependence of relaxation time (e) and modulus at G'=G'' (f) for 100% (○), 90% (□), 75% (◇), 50% (△) β-$C_{16}G_2$. (g) Cole-Cole plot for 100% (○), 90% (□), 75% (◇), 50% (△) β-$C_{16}G_2$ at 60 °C with a Maxwell model fit represented by the solid line.

surfactant concentration of 10 mM (Fig. S12). The same trend is observed for the contour length of the micelles obtained from a flexible cylinder model fit of the SANS data (Fig. 2b and c). Both these methods show a close to linear increase in size with increasing β-ratio, except at the highest ratios of β-$C_{16}G_2$, where the increase levels off. This may explain the sigmoidal zero-shear viscosity dependence on the surfactant ratio (Fig. 4a), where the trend micelle elongation reaches a plateau as seen by SANS and DLS. At high α-$C_{16}G_2$ ratios the surfactant micelles are shorter and correlate to the Newtonian behavior of the system.

Changing the temperature of the mixed solutions results in composition- and temperature-dependent variations in terms of micellar structure. For all compositions investigated here, the contour length obtained from SANS measurements is consistently *ca.* 1000 Å larger at 50 °C than 30 °C (Fig. 2c). This is in agreement with the variations in hydrodynamic radius obtained from DLS (Fig. S12). The onset of micelle growth with temperature is dependent on the surfactant ratio, where the onset occurs at lower temperatures for higher ratios of β-$C_{16}G_2$ (Fig. S13). In terms of variations in micellar flexibility with temperature, it is seen that, whilst the persistence length at 50 °C remains rather constant with micelle composition, micelle stiffness increases and becomes more variable at 30 °C (Fig. 2d). These structural features again correlate with the rheological behavior of the system, where more viscous systems are seen at 50 °C than at 30 °C. The scattering curves from the SANS data with the fitted flexible cylinder model and the obtained parameters is shown in Fig. S14 and Table S2.

In order to determine the internal structure of the micelles in the mixed-surfactant systems, contrast variation SANS was combined with SAXS. One of the main advantages of SANS is that the use of isotopically labelled compounds can provide detailed structural information and micelle composition through the co-refinement of model fits to the scattering data from these contrasts [32–34]. In addition to the SANS contrast presented above, protiated surfactants in D_2O (Contrast 1), analogous samples containing h-α-$C_{16}G_2$ and d_{31}-β-$C_{16}G_2$ in D_2O (Contrast 2) were measured. Data from this contrast were analyzed using a similar protocol to that presented in the Experimental section and ESI, with the difference that the volume fraction of micelles of Contrast 2 was fixed to the values obtained from Contrast 1 and the SLD of the micelle calculated (SLD_{fit}). SLD_{fit} was subsequently used to determine the amount of each surfactant in the micelle using Equation (5):

$$\varnothing_{\beta-C16G2,micelle} = \frac{SLD_{fit} - SLD_{h-C16}}{SLD_{d-C16} - SLD_{h-C16}} \quad (5)$$

where $\phi_{\beta\text{-C16G2,micelle}}$ is the volume fraction of β-$C_{16}G_2$ in the micelle, and $SLD_{h\text{-C16G2}}$ and $SLD_{d\text{-C16G2}}$ are the SLD of the protiated and deuterated surfactant tails, -0.39×10^{-6} Å^{-2} and 6.93×10^{-6} Å^{-2} respectively.

Data and results from the analysis are presented in Fig. S14 and Table S3 in the ESI. The results from Contrast 2 show similar structural characteristics to those obtained from Contrast 1. The main difference appears in the cross-sectional size of the micelles, where the radius is between 1 and 20% larger in the presence of d_{31}-β-$C_{16}G_2$ with respect to its protiated analogue. We are not sure about the reason of this difference. Interestingly, this difference does not seem to affect the elongation or flexibility of the micelles, as the differences between contrasts are within the error of the fits. The composition of the mixed micelles was determined at the two temperatures and shows that α-$C_{16}G_2$ is more prone to form micelles than β-$C_{16}G_2$ (Fig. S15). These results agree with previous investigations where it was shown that α-$C_{16}G_2$ has a lower CMC and thus relates to a more hydrophobic character [4,35]. SAXS data were used to determine the structural characteristics of the headgroup region, as the density correlation core–shell-solvent results in the strong oscillation at high q which enables the structure of this region to be depicted. Data and results from the analysis are presented in Fig. S16 and Table S4 in the ESI. In agreement with previous investigations, the cross-section thickness increases with increasing ratio of β-$C_{16}G_2$, which was attributed to the distinct differences in monomer packing that depends on the anomeric configuration of the surfactant [4].

4. Discussion

4.1. Comparison of $C_{16}G_2$ to other surfactants that form WLM

The results obtained for $C_{16}G_2$ in this study shows that only minor changes in the architecture of the surfactant have pronounced effect on micellar structure and rheology. Whilst the effect of changing the tail length or headgroup size of surfactant has been intensively studied [36], the effects of anomers have not been previously reported. The majority of studies on WLM were performed on ionic surfactant systems, especially when it comes to connection between rheology and micellar structure [5,37]. In particular, the addition of hydrotropic salts have a strong influence on the rheology of the system. An example is a 30 mM hexadecyltrimethylammonium tosylate solution where a zero-shear viscosity increases from around 10^{-2} Pas to about 50 Pas when potassium phthalic acid 2 mM was added [38]. Similarly,

the addition of sodium salicylate to 50 mM hexadecyltrimethylammonium chloride results in a strong non-Newtonian behavior, where the zero-shear viscosity increases to 10^4 Pas. These systems often require the presence of salts to form non-Newtonian fluids, which often are derived from aromatic hydrocarbons and thus present an adverse environmental impact.

The relationship between structure and rheological properties of non-ionic surfactants, such as sugar surfactants, is not as well understood as for other surfactant systems. The self-assembly structure of poly(oxyethylene) surfactants in solutions with non-Newtonian behavior has been shown to vary with the number of ethylene units in the headgroup [39]. Ericson *et al* also showed that for homologous series of maltosides and glucosides ($C_{14}G_2$, $C_{12}G_2$, $C_{10}G_1$, and C_9G_1) both size of head group and alkyl chain length affects the rheological properties and micellar structure formed [12–14]. The formation of non-Newtonian surfactant solutions was reported for β-$C_{14}G_2$, where the observed zero-shear viscosities were considerably lower than for the β-$C_{16}G_2$ solutions investigated here, with the highest zero-shear viscosity at 0.5 Pas for 18.5 wt% $C_{14}G_2$ solution. Despite the concentration of β-$C_{14}G_2$ being almost twice the highest concentration of β-$C_{16}G_2$ used in this study, the intersection between the viscous and elastic moduli occurs at a similar value (G', G'' ≈ 40 Pa) and the relaxation time is about two orders of magnitude higher for β-$C_{16}G_2$ at 200 mM (τ = 15 s) than for β-$C_{14}G_2$ at *ca.* 350 mM (τ = 0.03 s) [14]. This difference is attributed to the formation of more elongated and entangled micelles for β-$C_{16}G_2$.

To the best of the Author's knowledge, there are only two other sugar surfactant systems that have been reported to form viscoelastic solutions. These are sucrose monohexadecanoate [40,41], and a novel type of sugar surfactants with an ethylene oxide linker between the alkyl chain and the sugar headgroup as well as a double bond in the alkyl chain [11,42]. The sucrose monohexadecanoate showed a zero-shear viscosity of *ca.* 1 Pas for 10 wt% (172 mM) surfactant solutions, which is similar to the value obtained for a 100 mM 50% mixture of α- and β-$C_{16}G_2$ and almost three orders of magnitude lower than for a similar concentration of β-$C_{16}G_2$. The novel ethylene oxide-based sugar surfactants synthesized and studied by Moore *et al.* show a rheological behavior that is strongly dependent on the length of both head group and tail [11,42]. Interestingly, they also report the formation of WLM at a chain length of 16 carbons and above, which seems to be the tail length threshold above which alkylmaltopyranosides induce the type of viscoelastic behavior observed in the present study. Their results also showed that the differences in rheological behavior correlated with the structure of the sugar head group. The zero-shear viscosity for the surfactants with the highest viscosity, labelled as Gal-EO3-C18:1 and Glc-EO4-C22:1, was found to be 30 and 40 Pas at surfactant concentrations of 19.2 and 25.6 mM, respectively. These values are 1000 times higher than for β-$C_{16}G_2$ at 20 mM (0.02 Pas), i.e. these ethylene oxide-based sugar surfactant systems become more viscous at lower concentrations than β-$C_{16}G_2$. In contrast, the concentration of β-$C_{16}G_2$ needed to reach the same viscosity values is 70 mM. For 19.2 mM Glc-EO4-C22:1 the relaxation time was *ca.* 200 s, compared to *ca.* 15 s for 200 mM β-$C_{16}G_2$ at 40 °C [11]. This means that those surfactants form more elongated and entangled micelles than those of β-$C_{16}G_2$.

Additionally, the thermal stability of the non-Newtonian β-$C_{16}G_2$ solutions, where no clouding was observed up to 90 °C (Fig. S13), differs from that of poly(oxyethylene) surfactants, where high temperatures prompts system instability [43]. Therefore, the thermal resilience of the system allows to access a wide temperature range where the system remains stable.

5. Conclusions

The rheological behavior of aqueous systems can be tuned through the self-assembly of surfactants into worm-like micelles [5]. The formation of these assemblies has been previously reported for a variety of surfactants. Ionic surfactants often require the addition of salts or other surfactants to modify the monomer packing and lead to the co-assembly of those into elongated micelles [6–9,38]. In contrast, some non-ionic amphiphiles, e.g. poly(oxyethylene)-based surfactants, present the advantage of not requiring the addition of salts to form worm-like micelles, which simplifies the formulation of non-Newtonian fluids [10–11,42]. The molecular architecture of these (tail length and degree of headgroup polymerization) has been reported to control micelle morphology and, as such, the rheology of the system. Sugar-based surfactants have also been shown to self-assemble into micelles of different morphology depending on the monomer structure (tail length, degree of headgroup polymerization, and anomeric configuration), and worm-like micelles were also reported [4,12,14].

In this study, we present how the rheology of hexadecyl maltoside solutions is coupled to the microstructure of the system, with particular emphasis on the effect of the anomeric configuration of the surfactant (α and β). Surfactants in the α-configuration show a Newtonian behavior, in connection to the formation of globular or short cylindrical micelles in the whole concentration and temperature range studied here. For the β-configuration, we observed an increase of almost six orders of magnitude in viscosity with increasing concentration from the onset of the semi-dilute regime, at 10 mM, to the highest concentration investigated, 200 mM. These solutions were shear thinning and a distinct viscoelastic behavior was observed, where they behave as Maxwellian fluids at high concentrations. The structural characterization of the micelles in the dilute regime through scattering techniques shows the formation of WLM, which relates to the rheological behavior of the system upon entanglement, as previously reported for other systems [18,31,44,45]. Interestingly, it was also found that the temperature affects the rheological response of the system, where both the viscosity and the relaxation time go through a maximum with increasing temperature. These rheological properties are correlated to transitions in morphology and entanglement as induced by temperature changes. Interestingly, no phase separation was observed in the temperature range studied here. This confirms that the cloud point of the surfactant is higher than that for poly(oxyethylene)-based surfactants [43].

Furthermore, when mixing these two surfactants, the rheological properties fall between those of the two pure anomers, in connection to the microscopic structure. At higher β-$C_{16}G_2$ content, micelles are longer and, potentially, more entangled in the semi-dilute regime. This explains the increase in viscosity and why the elastic modulus is dominating over a larger timeframe, showing that mixtures of these surfactants allow to finely tune the system's response to stress.

Interestingly, one of the key features for these $C_{16}G_2$-systems is how the behavior of two surfactants of identical chemical composition can differ so greatly by altering the anomeric configuration, which to the best of our knowledge has not been previously reported for this type of systems. Furthermore, the green character of these, which can be synthesized using renewable raw materials, opens new possibilities in the use of sustainable surfactants as rheology modifiers for formulated products. Therefore, increasing the physicochemical understanding of these surfactants and exploring other conditions (e.g. formation of liquid crystals at high surfactant concentration) will expand the application of these to replace fossil fuel-derived compounds.

CRediT authorship contribution statement

Johan Larsson: Conceptualization, Methodology, Investigation, Formal analysis, Writing - original draft, Writing - review & editing, Visualization. **Adrian Sanchez-Fernandez:** Conceptualization, Methodology, Investigation, Formal analysis, Writing - original draft, Writing - review & editing, Visualization. **Anna Leung:** Investigation, Resources, Writing - review & editing. **Ralf Schweins:** Investigation, Resources, Writing - review & editing. **Baohu Wu:** Investigation, Resources. **Tommy Nylander:** Conceptualization, Investigation, Writing - review & editing, Funding acquisition. **Stefan Ulvenlund:** Conceptualization, Investigation, Writing - review & editing, Funding acquisition. **Marie Wahlgren:** Conceptualization, Methodology, Investigation, Writing - original draft, Writing - review & editing, Funding acquisition.

Declaration of Competing Interest

The authors declare that they have no known competing financial interests or personal relationships that could have appeared to influence the work reported in this paper.

Acknowledgements

The authors are also thankful to Swedish Research Council Formas (Grant 2015-666) for the funding for J.L. The research in this study was performed with financial support from Vinnova - Swedish Governmental Agency for Innovation Systems within the NextBioForm Competence Centre. This work is based upon experiments performed on the KWS-3 instrument, operated by JCNS at the Heinz Maier-Leibnitz Zentrum (MLZ), Garching, Germany (Proposal No. 15556), and on the D11 instrument at the Institute Laue-Langevin, Grenoble, France (Proposal No. 9-10-1587). Experimental data from the D11 experiment has been made freely available at DOI:10.5291/ILL-DATA.9-10-1587. The SAXS experiments were performed on beamline BM29 at the European Synchrotron Radiation Facility (ESRF), Grenoble, France. We are grateful to Dr Martha Brennich at the ESRF for providing assistance in using the beamline. This work benefited from the use of the SasView application, originally developed under NSF award DMR-0520547. SasView contains code developed with funding from the European Union's Horizon 2020 research and innovation programme under the SINE2020 project, grant agreement No 654000.

Appendix A. Supplementary material

Supplementary data to this article can be found online at https://doi.org/10.1016/j.jcis.2020.08.116.

References

[1] R. Lebeuf, C.-Y. Liu, C. Pierlot, V. Nardello-Rataj, Synthesis and surfactant properties of nonionic biosourced alkylglucuronamides, ACS Sustainable Chem. Eng. 6 (2) (2018) 2758–2766.
[2] D. Balzer, H. Lüders, Nonionic Surfactants: Alkyl Polyglucosides, Marcel Dekker, New York, 2000.
[3] A.M. Seddon, P. Curnow, P.J. Booth, Membrane proteins, lipids and detergents: not just a soap opera, Biochim. Biophys. Acta (BBA) – Biomembr. 1666 (1) (2004) 105–117.
[4] J. Larsson, A. Sanchez-Fernandez, N. Mahmoudi, L.C. Barnsley, M. Wahlgren, T. Nylander, S. Ulvenlund, Effect of the anomeric configuration on the micellization of hexadecylmaltoside surfactants, Langmuir 35 (43) (2019) 13904–13914.
[5] C.A. Dreiss, Wormlike micelles: where do we stand? Recent developments, linear rheology and scattering techniques, Soft Matter 3 (8) (2007) 956–970.
[6] G. Porte, J. Appell, Y. Poggi, Experimental investigations on the flexibility of elongated cetylpyridinium bromide micelles, J. Phys. Chem. 84 (23) (1980) 3105–3110.
[7] L.J. Magid, Z. Li, P.D. Butler, Flexibility of elongated sodium dodecyl sulfate micelles in aqueous sodium chloride: a small-angle neutron scattering study, Langmuir 16 (26) (2000) 10028–10036.
[8] N.C. Das, H. Cao, H. Kaiser, G.T. Warren, J.R. Gladden, P.E. Sokol, Shape and size of highly concentrated micelles in CTAB/NaSal solutions by small angle neutron scattering (SANS), Langmuir 28 (33) (2012) 11962–11968.
[9] P.A. Hassan, S.R. Raghavan, E.W. Kaler, Microstructural changes in SDS micelles induced by hydrotropic salt, Langmuir 18 (7) (2002) 2543–2548.
[10] G. Jerke, J.S. Pedersen, S.U. Egelhaaf, P. Schurtenberger, Flexibility of charged and uncharged polymer-like micelles, Langmuir 14 (21) (1998) 6013–6024.
[11] J.E. Moore, T.M. McCoy, A.V. Sokolova, L. de Campo, G.R. Pearson, B.L. Wilkinson, R.F. Tabor, Worm-like micelles and vesicles formed by alkyl-oligo (ethylene glycol)-glycoside carbohydrate surfactants: the effect of precisely tuned amphiphilicity on aggregate packing, J. Colloid Interface Sci. 547 (2019) 275–290.
[12] C.A. Ericsson, O. Söderman, V.M. Garamus, M. Bergström, S. Ulvenlund, Effects of temperature, salt, and deuterium oxide on the self-aggregation of alkylglycosides in dilute solution. 2. n-Tetradecyl-beta-D-maltoside, Langmuir: ACS J. Surf. Colloids 21 (4) (2005) 1507–1515.
[13] C.A. Ericsson, O. Söderman, V.M. Garamus, M. Bergström, S. Ulvenlund, Effects of temperature, salt, and deuterium oxide on the self-aggregation of alkylglycosides in dilute solution. 1. n-nonyl-β-d-glucoside, Langmuir 20 (4) (2004) 1401–1408.
[14] C.A. Ericsson, O. Söderman, S. Ulvenlund, Aggregate morphology and flow behaviour of micellar alkylglycoside solutions, Colloid Polym. Sci. 283 (12) (2005) 1313–1320.
[15] A.C. Williams, B.W. Barry, Penetration enhancers, Adv. Drug Deliv. Rev. 56 (5) (2004) 603–618.
[16] B. Kronberg, K. Holmberg, B. Lindman, Surface Chemistry of Surfactants and Polymers, John Wiley & Sons Ltd, 2014.
[17] P.-G. De Gennes, Scaling Concepts in Polymer Physics, Cornell University Press, 1979.
[18] B.A. Schubert, E.W. Kaler, N.J. Wagner, The microstructure and rheology of mixed cationic/anionic wormlike micelles, Langmuir 19 (10) (2003) 4079–4089.
[19] M. Cates, Reptation of living polymers: dynamics of entangled polymers in the presence of reversible chain-scission reactions, Macromolecules 20 (9) (1987) 2289–2296.
[20] J.F. Berret, J. Appell, G. Porte, Linear rheology of entangled wormlike micelles, Langmuir 9 (11) (1993) 2851–2854.
[21] S. Ezrahi, E. Tuval, A. Aserin, Properties, main applications and perspectives of worm micelles, Adv. Colloid Interface Sci. 128–130 (2006) 77–102.
[22] M.E. Cates, S.J. Candau, Statics and dynamics of worm-like surfactant micelles, J. Phys.: Condens. Matter 2 (33) (1990) 6869–6892.
[23] S.R. Midtgaard, T.A. Darwish, M.C. Pedersen, P. Huda, A.H. Larsen, G.V. Jensen, S.A.R. Kynde, N. Skar-Gislinge, A.J.Z. Nielsen, C. Olesen, M. Blaise, J.J. Dorosz, T. S. Thorsen, R. Venskutonytė, C. Krintel, J.V. Møller, H. Frielinghaus, E.P. Gilbert, A. Martel, J.S. Kastrup, P.E. Jensen, P. Nissen, L. Arleth, Invisible detergents for structure determination of membrane proteins by small-angle neutron scattering, FEBS J. 285 (2) (2018) 357–371.
[24] P. Pernot, A. Round, R. Barrett, A. De Maria Antolinos, A. Gobbo, E. Gordon, J. Huet, J. Kieffer, M. Lentini, M. Mattenet, C. Morawe, C. Mueller-Dieckmann, S. Ohlsson, W. Schmid, J. Surr, P. Theveneau, L. Zerrad, S. McSweeney, Upgraded ESRF BM29 beamline for SAXS on macromolecules in solution, J. Synchrot. Radiat. 20 (4) (2013) 660–664.
[25] K. Lieutenant, P. Lindner, R. Gahler, A new design for the standard pinhole small-angle neutron scattering instrument D11, J. Appl. Crystallogr. 40 (6) (2007) 1056–1063.
[26] V. Pipich, Z. Fu, KWS-3: Very small angle scattering diffractometer with focusing mirror, J. Large-Scale Res. Facil. JLSRF 1 (A31) (2015).
[27] M.C. Doucet, Jae Hie, Alina, Gervaise, Bakker, Jurrian, Bouwman, Wim, Butler, Paul, Campbell, Kieran, Gonzales, Miguel, Heenan, Richard, Jackson, Andrew, Juhas, Pavol, King, Stephen, Kienzle, Paul, Krzywon, Jeff, Markvardsen, Anders, Nielsen, Torben, O'Driscoll, Lewis, Potrzebowski, Wojciech, Ferraz Leal, Ricardo, Richter, Tobias, Rozycko, Piotr, Snow, Tim, Washington, Adam SasView version 4.2.2. https://doi.org/10.5281/zenodo.2652478.
[28] M. Cates, Dynamics of living polymers and flexible surfactant micelles: scaling laws for dilution, J. Phys. 49 (9) (1988) 1593–1600.
[29] J.S. Pedersen, P. Schurtenberger, Scattering functions of semiflexible polymers with and without excluded volume effects, Macromolecules 29 (23) (1996) 7602–7612.
[30] W.-R. Chen, P.D. Butler, L.J. Magid, Incorporating intermicellar interactions in the fitting of SANS data from cationic wormlike micelles, Langmuir 22 (15) (2006) 6539–6548.
[31] R.D. Koehler, S.R. Raghavan, E.W. Kaler, Microstructure and dynamics of wormlike micellar solutions formed by mixing cationic and anionic surfactants, J. Phys. Chem. B 104 (47) (2000) 11035–11044.
[32] P.A. Hassan, G. Fritz, E.W. Kaler, Small angle neutron scattering study of sodium dodecyl sulfate micellar growth driven by addition of a hydrotropic salt, J. Colloid Interface Sci. 257 (1) (2003) 154–162.
[33] J.S. Pedersen, Analysis of small-angle scattering data from colloids and polymer solutions: modeling and least-squares fitting, Adv. Colloid Interface Sci. 70 (1997) 171–210.
[34] M. Bergström, J. Skov Pedersen, Structure of pure SDS and DTAB micelles in brine determined by small-angle neutron scattering (SANS), PCCP 1 (18) (1999) 4437–4446.

[35] F. Nilsson, O. Söderman, I. Johansson, Four different C8G1 alkylglucosides. anomeric effects and the influence of straight vs branched hydrocarbon chains, J. Colloid Interface Sci. 203 (1998) 131–139.
[36] K.D. Danov, P.A. Kralchevsky, S.D. Stoyanov, J.L. Cook, I.P. Stott, E.G. Pelan, Growth of wormlike micelles in nonionic surfactant solutions: quantitative theory vs. experiment, Adv. Colloid Interface Sci. 256 (2018) 1–22.
[37] L.M. Walker, Rheology and structure of worm-like micelles, Curr. Opin. Colloid Interface Sci. 6 (5) (2001) 451–456.
[38] K.N. Silva, R. Novoa-Carballal, M. Drechsler, A.H.E. Müller, E.K. Penott-Chang, A. J. Müller, The influence of concentration and pH on the structure and rheology of cationic surfactant/hydrotrope structured fluids, Colloids Surf., A 489 (2016) 311–321.
[39] P.G. Cummins, E. Staples, J. Penfold, R.K. Heenan, The geometry of micelles of the poly(oxyethylene) nonionic surfactants C16E6 and C16E8 in the presence of electrolyte, Langmuir 5 (5) (1989) 1195–1199.
[40] K. Aramaki, S. Hoshida, S. Arima, Effect of carbon chain length of cosurfactant on the rheological properties of nonionic wormlike micellar solutions formed by a sugar surfactant and monohydroxy alcohols, Colloids Surf., A 366 (1) (2010) 58–62.
[41] H. Kunieda, C. Rodriguez, Y. Tanaka, M.H. Kabir, M. Ishitobi, Effects of added nonionic surfactant and inorganic salt on the rheology of sugar surfactant and CTAB aqueous solutions, Colloids Surf., B 38 (3) (2004) 127–130.
[42] J.E. Moore, T.M. McCoy, L. de Campo, A.V. Sokolova, C.J. Garvey, G. Pearson, B.L. Wilkinson, R.F. Tabor, Wormlike micelle formation of novel alkyl-tri(ethylene glycol)-glucoside carbohydrate surfactants: structure–function relationships and rheology, J. Colloid Interface Sci. 529 (2018) 464–475.
[43] P.O. Cummins, J.B. Hayter, J. Penfold, E. Staples, A small-angle neutron scattering investigation of shear-aligned hexaethyleneglycolmonohexadecylether (C16E6) micelles as a function of temperature, Chem. Phys. Lett. 138 (5) (1987) 436–440.
[44] B.F. García, S. Saraji, A new insight into the dependence of relaxation time on frequency in viscoelastic surfactant solutions: From experimental to modeling study, J. Colloid Interface Sci. 517 (2018) 265–277.
[45] W. Zou, G. Tan, H. Jiang, K. Vogtt, M. Weaver, P. Koenig, G. Beaucage, R.G. Larson, From well-entangled to partially-entangled wormlike micelles, Soft Matter 15 (4) (2019) 642–655.